Observation of Quantum Jumps in a Superconducting Artificial Atom

R. Vijay, D. H. Slichter, and I. Siddiqi

Quantum Nanoelectronics Laboratory, Department of Physics, University of California, Berkeley, California 94720, USA

(Received 29 September 2010; published 14 March 2011)

We continuously measure the state of a superconducting quantum bit coupled to a microwave readout cavity by using a fast, ultralow-noise parametric amplifier. This arrangement allows us to observe quantum jumps between the qubit states in real time, and should enable quantum error correction and feedback—essential components of quantum information processing.

DOI: 10.1103/PhysRevLett.106.110502 PACS numbers: 03.67.Lx, 42.50.Lc, 42.50.Pq, 85.25.−j

A continuously monitored quantum system prepared in an excited state will decay to its ground state with an abrupt jump. The jump occurs stochastically on a characteristic time scale T_1, the lifetime of the excited state, provided the measurement is not too strong. Such quantum jumps, originally envisioned by Bohr, have been observed in trapped atoms and ions [1–3], single molecules [4], photons [5], single electrons in cyclotrons [6], microscopic defects in a Josephson junction [7], and recently in nuclear [8] and electron [9] spins. Observation of quantum jumps requires a quantum nondemolition (QND) measurement scheme, that is, one which leaves the system in an eigenstate of the measured observable [10], thus allowing repeated measurements. One must also be able to perform the measurements on a time scale much faster than T_1 in order to resolve the jumps. All previous experiments have used microscopic quantum degrees of freedom with long relaxation times ($\sim$ ms to s).

Superconducting quantum bits (qubits) [11] exploit macroscopic quantum degrees of freedom in an electrical circuit and typically have much shorter relaxation times ($\sim \mu$s) on account of strong coupling to their environment. However, they are easy to manipulate, tunable and can be mass produced, making them a promising candidate for a scalable quantum computing architecture. Moreover, the drawbacks of short relaxation times can be overcome by using quantum error correction [12] which requires a fast, high-fidelity measurement scheme. Further, if the measurement is QND, one can use feedback techniques to perform continuous error correction [13]; to date, though, no suitable measurement scheme has been demonstrated.

In this Letter, we report the first observation of quantum jumps in a superconducting qubit—a macroscopic quantum system—by implementing a high-fidelity, QND measurement scheme using a fast, ultralow-noise parametric amplifier [14]. Our experiment uses the circuit quantum electrodynamics (cQED) architecture, where the superconducting qubit is dispersively coupled to a superconducting cavity [15], in analogy to an atom in a Fabry-Perot cavity. Probing the qubit-state-dependent cavity frequency implements a continuous, high visibility QND measurement [16].

Despite successfully demonstrating QND measurement with several kinds of superconducting qubits [17–19], cQED implementations with linear cavities have typically suffered from low single-shot fidelity, precluding the observation of quantum jumps. This is primarily due to inefficient amplification of the photons leaving the cavity. The noise added by state-of-the-art cryogenic semiconductor microwave amplifiers is considerably larger than the signal from the cavity, necessitating repeated measurements to resolve the qubit state [16]. Using more readout photons can induce qubit state mixing [20], thus limiting the fidelity. Other high-fidelity readout schemes implemented for superconducting qubits are either too slow [21] or are not QND [22]. Josephson parametric amplifiers [23,24] with near quantum limited noise performance can potentially enable single-shot readout in the cQED architecture, but most existing designs have an instantaneous bandwidth below 1 MHz, too small to enable real-time monitoring of the qubit state. Since superconducting qubit lifetimes are typically around 1 μs, one would need a bandwidth of order 10 MHz to resolve quantum jumps between qubit states with high fidelity. We achieve this by using a low quality factor (Q) nonlinear resonator operated as a parametric amplifier [14,25].

Our experimental setup, shown schematically in Fig. 1, is anchored to the mixing chamber of a dilution refrigerator at 30 mK. The superconducting readout cavity (brown) is implemented as a quasi-lumped element linear resonator [26] consisting of a meander inductor ($L = 1.25$ nH) in parallel with an interdigitated capacitor ($C = 575$ fF). A transmon qubit [27] (blue, $E_J = 11.4$ GHz, $E_C = 280$ MHz) is capacitively coupled to the cavity. This arrangement is different than typical cQED setups which use transmission line resonators for the cavity. This design has a smaller footprint and avoids detrimental higher cavity modes [18]. Probe photons enter from the input port and reflect off the readout cavity, acquiring a phase shift that depends on the qubit state. These photons then travel through a series of circulators, which allow microwave signals to propagate in one direction as indicated by the arrows in the figure, to the parametric amplifier (paramp), which amplifies the signal and sends it to the

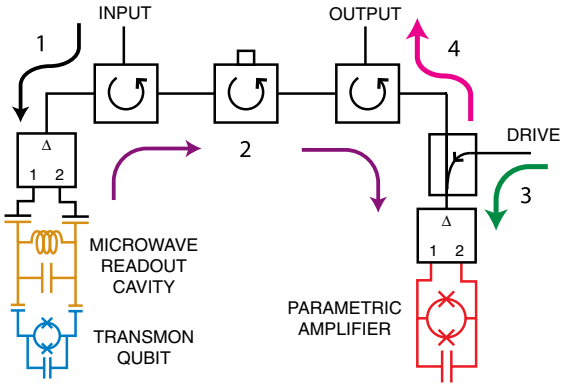

FIG. 1 (color online). Experimental setup. Readout photons (black arrow, "1") enter from the input port and are directed through a microwave circulator to a 180° hybrid, which converts the single-ended microwave signal into a differential one. The photons interact with the readout cavity and the reflected signal (purple arrows, "2") carries information about the qubit state toward the parametric amplifier (paramp) through three circulators, which isolate the readout and qubit from the strong pump of the paramp. A directional coupler combines this signal with pump photons (green arrow, "3") from the drive port. The paramp amplifies the readout signal, and the amplified signal (magenta arrow, "4") is reflected and sent through the third circulator to the output port. Qubit manipulation pulses are also sent via the input port.

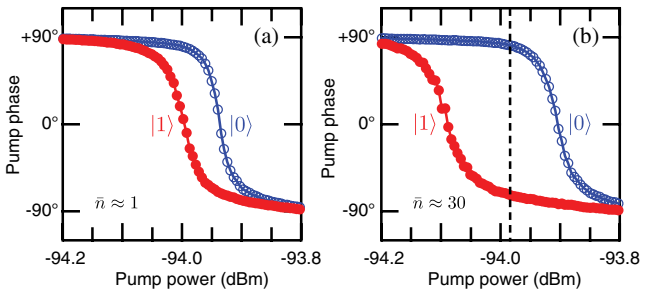

FIG. 2 (color online). Parametric amplifier response. In (a), we plot the measured average phase of the reflected pump as a function of pump power with the qubit prepared in the ground (blue, open circles) or excited (red, solid circles) states and an average readout cavity occupation of about one photon. Panel (b) shows the same curves for higher average photon number ($\bar{n} \approx 30$) in the readout cavity, which increases the relative separation. The vertical dashed line shows the optimal bias point.

output port. The signal is further amplified by cryogenic and room temperature amplifiers before being mixed down to zero frequency, digitized, and recorded.

The bare readout cavity frequency is 5.923 GHz, with a linewidth $\kappa/2\pi = 4.9$ MHz. The qubit frequency is set at 4.753 GHz, corresponding to a detuning $\Delta/2\pi = 1.170$ GHz. The cavity is driven at 5.932 GHz (the cavity frequency corresponding to the qubit in the ground state), and we define $\bar{n} = (\bar{n}_g + \bar{n}_e)/2$, where $\bar{n}_g$ and $\bar{n}_e$ are the average readout cavity occupations at a given excitation power with the qubit in the ground and excited states, respectively. These occupations are calibrated using the ac Stark effect for a multilevel qubit [25]. The measured coupling strength $g/2\pi = 109$ MHz results in a dispersive shift of the cavity [27] due to the qubit state $2\chi/2\pi = 4.3$ MHz. We measure qubit lifetime $T_1 = 320$ ns and dephasing time $T_2^* = 290$ ns at this qubit operating point.

When the paramp is appropriately biased with a strong pump tone, the reflected pump has a power-dependent phase shift as shown in Fig. 2. Since the phase changes sharply with pump power, a small change in the pump power due to an additional signal at the pump frequency is amplified into a large phase shift on the pump signal. This mode of operation only amplifies signals in phase with the pump signal and theoretically adds no noise [28], maintaining the signal-to-noise ratio (SNR) of the input signal. If the noise on the input signal is only due to quantum fluctuations, then the noise floor can be expressed as a noise temperature $T_Q = \hbar\omega_s/2k_B \approx 142$ mK, where $\omega_s/2\pi = 5.932$ GHz is the signal frequency. By contrast, typical microwave amplification chains have a system noise temperature in the range 10–30 K, about 2 orders of magnitude higher. Near noiseless operation, along with large bandwidth, was previously demonstrated for this paramp design [14].

Since $2\chi \approx \kappa$, measurement photons at 5.932 GHz exiting the readout cavity will have a relative phase shift of about 180°, depending on the state of the qubit. When these photons arrive at the paramp, they coherently add to or subtract from the pump (also at 5.932 GHz, and tuned to be in phase with the readout photons), causing a phase shift of up to 180° in the reflected pump photons which form the output signal. This can be seen in Fig. 2(a), where the average phase of the output signal is plotted as a function of pump power. The two traces correspond to measurements taken with the qubit prepared in the ground (blue, open circles) and excited (red, solid circles) states, with $\bar{n} \approx 1$ photon. Increasing the number of photons in the cavity further separates the ground and excited state curves as shown in Fig. 2(b) for $\bar{n} \approx 30$ photons. This level of excitation of the readout cavity maximizes readout SNR while keeping the measurement QND, and was used for all further measurements discussed below.

With this technique, we can perform single-shot measurements of the qubit state and observe quantum jumps. We prepare the qubit state with a 20 ns pulse of varying amplitude at the qubit frequency of 4.753 GHz and immediately probe the cavity with photons at 5.932 GHz. The amplified signal is then mixed down to zero frequency, effectively converting the phase shift signal of the readout into a single-quadrature voltage signal. This voltage is then digitized at 10 ns intervals. Figure 3(a) shows the pulse sequence and Fig. 3(b) plots 20 individual traces for each of three pulse amplitudes corresponding to 0, π, and 2π qubit rotations. We discriminate between ground and

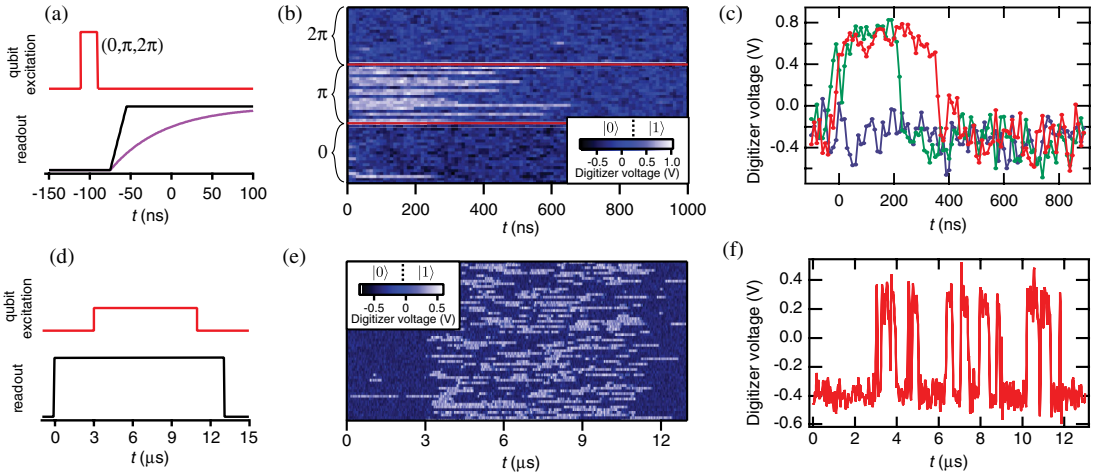

FIG. 3 (color online). Quantum jumps. (a) shows the pulse sequence used to generate (b) and (c). The qubit is excited with a pulse of varying amplitude (red), and the readout (black) is immediately energized, causing the cavity population (purple) to rise and effect a measurement. Time $t = 0$ corresponds to two cavity time constants after the readout is energized. (b) shows 20 representative single-shot traces for three different qubit rotations (0, π, and 2π). Abrupt quantum jumps from the excited state (white) to the ground state (blue) are clearly visible for the data corresponding to the π pulse, while the traces corresponding to 0 and 2π indicate that the qubit is mostly in the ground state. (c) shows single-shot time traces following a π (red and green) and 2π (blue) pulse. (d) shows the pulse sequence used to generate (e) and (f). Here the readout is energized with the qubit in the ground state, and then a continuous qubit drive is applied after a 3 μs delay. (e) and (f) show 60 traces and one trace, respectively, of the qubit jumping between the ground and excited state under the influence of both the qubit drive and measurement pinning.

excited states using a threshold level of 0.25 V, as indicated on the scale bar. One can clearly see abrupt quantum jumps from the excited state (white) to the ground state (blue) for the data corresponding to a π pulse, while the traces corresponding to 0 and 2π show the qubit mostly in the ground state. A few traces after 0 and 2π pulses show jumps to the excited state, and a few traces after a π pulse are never measured to be in the excited state. We attribute the first effect to qubit state mixing due to high photon numbers in the readout cavity [20], and the second effect to the qubit spontaneously decaying before the cavity can ramp up [16]. Three representative traces of the quantum jumps are shown in Fig. 3(c), one where the qubit was prepared in the ground state (blue) and two where it was prepared in the excited state (red and green) and subsequently relaxed to the ground state at different times. The SNR in the measured traces is defined as $\mathrm{SNR}_{\mathrm{meas}} = |\mu_g - \mu_e|/(\sigma_g + \sigma_e)$ where (μ_g, μ_e) and (σ_g, σ_e) are the mean and standard deviation of the digitizer voltages corresponding to the ground and excited states, respectively. We measure an SNR of about 3.75, a factor of 2.3 lower than the theoretical value of $\sqrt{\bar{n}_g \kappa/B} = 8.5$, where $B = 20$ MHz is our measurement bandwidth. We attribute this discrepancy primarily to saturation of the paramp at this high readout power; details are discussed in the supplementary information [25].

We also investigated the effect of simultaneous qubit excitation and measurement. We energize the readout and then turn on a long qubit excitation pulse after a few μs, as shown in Fig. 3(d). This qubit drive tries to coherently change the qubit state while the projective measurement forces the qubit to be in the ground or excited state, resulting in the random telegraph signal seen in Figs. 3(e) and 3(f). Note that the discrimination threshold here (-0.05 V) is different than that in Figs. 3(b) and 3(c) due to different bias conditions for the paramp. Previous measurements [29] have only been able to indirectly infer such quantum jumps from the averaged spectrum of the measurement signal. This inhibition of qubit state evolution due to measurement is the essence of the quantum Zeno effect [30,31] and will be the subject of future work using samples with longer coherence times and further improvements in measurement signal-to-noise ratio.

Finally, we look at the statistics of these quantum jumps. Figure 4(a) plots a histogram of 2×10^4 individual measurements with the qubit prepared in the excited state, as a function of digitizer voltage and time [32]. Most of the population is measured in the excited state (centered around 0.6 V) at $t = 0$ and then decays to the ground state (centered around -0.3 V) with a time constant $\tau = 290$ ns [Fig. 4(b), inset]. Despite the large separation between the ground and excited state peaks, the maximum qubit readout fidelity is about 70%. This can be almost entirely attributed to the measured $T_1 = 320$ ns being comparable to the cavity rise time $2/\kappa = 65$ ns, which means that around 30% of the excited state population decays to the ground state before the measurement is made. Since we can resolve individual decay events, we can also plot a

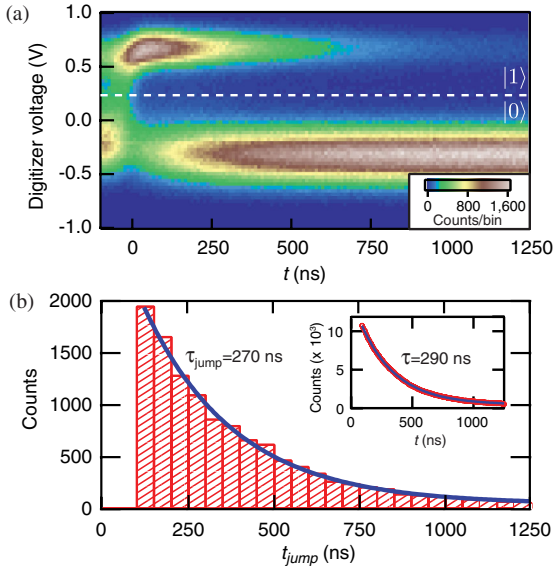

FIG. 4 (color online). Jump statistics. (a) shows a histogram of 2×10^4 individual measurements with the qubit prepared with a π pulse and $\bar{n} \approx 30$ readout photons. The excited state signal, centered around 0.6 V, is clearly resolved from the ground state signal at -0.3 V; the dashed line shows the discrimination threshold. The ensemble population is predominately in the excited state at $t = 0$, and decays to the ground state with a time constant [(b), inset] $\tau = 290$ ns. (b) shows a histogram of jump times from the excited state to the ground state extracted from individual measurements. The solid line is an exponential fit with a time constant $\tau_{\mathrm{jump}} = 270$ ns. We do not plot jumps that occur less than two cavity time constants after the readout is energized. The pulse protocol used is shown in Fig. 3(a).

histogram of the jump (excited to ground state) times [33] as shown in Fig. 4(b). The histogram shows an exponential decay with a time constant $\tau_{\mathrm{jump}} = 270$ ns. Both these time constants are consistent with each other and with the measured T_1 of the qubit, as would be expected for a QND measurement [20].

In conclusion, we have demonstrated high-fidelity, real-time monitoring of a superconducting qubit and observed quantum jumps in this macroscopic quantum system. This is the first fruit of a powerful technique for quantum measurements in solid state systems and is a major step toward implementing quantum feedback control and quantum error correction. Our measurement technique can be readily extended to a variety of other systems of interest, including nitrogen vacancy centers in diamond and lower-dimensional semiconductor systems. Furthermore, our work suggests a route to study the quantum Zeno effect [31] and to shed further light on nonidealities in quantum measurement processes [20]. The high-fidelity quantum measurements we have demonstrated can also be used to realize a time-resolved single microwave photon source or detector [31], thus enabling a new class of quantum optics experiments in the solid state.

We thank M. H. Devoret, R. J. Schoelkopf, J. Gambetta, M. Hatridge and O. Naaman for useful discussions. R. V. and I. S. acknowledge funding from AFOSR under Grant No. FA9550-08-1-0104. D. H. S. acknowledges support from a Hertz Foundation Fellowship endowed by Big George Ventures.

[1] W. Nagourney, J. Sandberg, and H. Dehmelt, Phys. Rev. Lett. **56**, 2797 (1986).
[2] J. C. Bergquist *et al.*, Phys. Rev. Lett. **57**, 1699 (1986).
[3] T. Sauter *et al.*, Phys. Rev. Lett. **57**, 1696 (1986).
[4] T. Basche, S. Kummer, and C. Brauchle, Nature (London) **373**, 132 (1995).
[5] S. Gleyzes *et al.*, Nature (London) **446**, 297 (2007).
[6] S. Peil and G. Gabrielse, Phys. Rev. Lett. **83**, 1287 (1999).
[7] Y. Yu *et al.*, Phys. Rev. Lett. **101**, 157001 (2008).
[8] P. Neumann *et al.*, Science **329**, 542 (2010).
[9] A. N. Vamivakas *et al.*, Nature (London) **467**, 297 (2010).
[10] V. B. Braginsky and F. Y. Khalili, Rev. Mod. Phys. **68**, 1 (1996).
[11] J. Clarke and F. K. Wilhelm, Nature (London) **453**, 1031 (2008).
[12] P. W. Shor, Phys. Rev. A **52**, R2493 (1995).
[13] C. Ahn, A. C. Doherty, and A. J. Landahl, Phys. Rev. A **65**, 042301 (2002).
[14] M. Hatridge, R. Vijay, D. H. Slichter, J. Clarke, and I. Siddiqi, arXiv:1003.2466.
[15] A. Blais *et al.*, Phys. Rev. A **69**, 062320 (2004).
[16] A. Wallraff *et al.*, Phys. Rev. Lett. **95**, 060501 (2005).
[17] A. Wallraff *et al.*, Nature (London) **431**, 162 (2004).
[18] A. A. Houck *et al.*, Phys. Rev. Lett. **101**, 080502 (2008).
[19] V. E. Manucharyan *et al.*, Science **326**, 113 (2009).
[20] M. Boissonneault, J. M. Gambetta, and A. Blais, Phys. Rev. A **79**, 013819 (2009).
[21] F. Mallet *et al.*, Nature Phys. **5**, 791 (2009).
[22] J. M. Martinis, Quant. Info. Proc. **8**, 81 (2009).
[23] M. A. Castellanos-Beltran *et al.*, Nature Phys. **4**, 929 (2008).
[24] N. Bergeal *et al.*, Nature (London) **465**, 64 (2010).
[25] See supplemental material at http://link.aps.org/supplemental/10.1103/PhysRevLett.106.110502 for details on photon number calibration, paramp operation and fabrication.
[26] M. S. Khalil, F. C. Wellstood, and K. D. Osborn, arXiv:1008.2929.
[27] J. Koch *et al.*, Phys. Rev. A **76**, 042319 (2007).
[28] C. M. Caves, Phys. Rev. D **26**, 1817 (1982).
[29] A. Palacios-Laloy *et al.*, Nature Phys. **6**, 442 (2010).
[30] W. M. Itano *et al.*, Phys. Rev. A **41**, 2295 (1990).
[31] J. Gambetta *et al.*, Phys. Rev. A **77**, 012112 (2008).
[32] See supplemental material at http://link.aps.org/supplemental/10.1103/PhysRevLett.106.110502 which shows a movie of the evolution of the histogram as a function of qubit Rabi drive strength.
[33] See supplemental material at http://link.aps.org/supplemental/10.1103/PhysRevLett.106.110502 which shows a movie of the evolution of this histogram as it builds up.